NASA-CR-202814

Unsteady Spherical Flames in Dusty Gases

J. Buckmaster and A. Agarwal
University of Illinois, Urbana, IL 61801

Corresponding author:
J. Buckmaster
Department of Aeronautical and Astronautical Engineering
The University of Illinois
321 Talbot Laboratory
104 South Wright Street
Urbana, IL 61801, USA
tel: 217.333.1803 fax: 217.244.0720 internet: LIMEY@UXH.CSO.UIUC.EDU

After January 1, 1994:
Department of Mathematics
Hong Kong University of Science and Technology
Clear Water Bay
Kowloon, Hong Kong
tel: 852.358.7412 fax: 852.358.1643 internet: LIMEY@UXH.CSO.UIUC.EDU

Word Count: words (machine count) 3626; equation equivalent 651;
1 table 200; 6 figures 1200; TOTAL 5677

Prefer oral presentation with publication in the Proceedings

Theory (3.4) (3.8) Premixed Laminar Flames - Radiation Effects

Abstract

We examine an expanding spherical premixed flame propagating in a mixture containing inert dust. The presence of the dust generates a significant radiative energy flux that influences the flame speed. With the adoption of a hydrodynamic description in which stretch effects are accounted for using an empirical formula, and with the use of the Eddington approximation to describe the radiation, a simple numerical problem is formulated valid for that initial time interval in which the flame-temperature changes by $O(\varepsilon)$ amounts where ε is the small inverse activation energy. Solutions are constructed using parameter values appropriate to lean CH_4/air mixtures, and for modest particle loadings. We describe the competition between the *Spalding effect* in which radiative losses on the diffusive scale tend to quench the flame, and the *Joulin effect* in which radiative preheating on the scale of the Planck length tends to strengthen the flame.

Introduction

The present paper is concerned with a theoretical study of unsteady spherical flames generated by point ignition and propagating in mixtures containing inert dust. The presence of particles in the mixture can have a variety of effects, but in this early work we wish to focus solely on the radiation field that is generated, together with its energetic consequences. Past theoretical work has concentrated on the plane geometry (e.g. [1]), but the spherical geometry is better suited for experimental study. At the present time complete quantitative experimental data is not available, but an experimental program is planned [2] and we believe that there is need for concurrent theoretical work to help define experimental strategies and to identify the physics responsible for the observed phenomena.

Consider a pencil of radiation of intensity I defined by an element of solid angle $\delta\Omega$. The element of volume $\delta V = \delta\Omega\, r^2\, \delta r$ contains $N\, \delta\Omega\, r^2\, \delta r$ particles, where N is the particle number density. If each particle is assumed to be a sphere of diameter d, the fraction of the pencil intercepted by the particles is $(\pi d^2/4)\, N\delta\Omega r^2 \delta r / \delta\Omega r^2 = (\pi d^2/4)\; N\, \delta r$. Thus

$$dI/dr = -(\pi d^2/4)\; N\; I(r) \equiv -I(r)/l \qquad (1)$$

where $l = 4/N\pi d^2$ is the absorption length. If ρ_s is the bulk solid density, ρ the gas density, and τ the density of a single particle, then

$$l/d = (2/3)(\tau/\rho)(\rho/\rho_s)\;. \qquad (2)$$

When the particles are small enough they will have a speed identical to that of the gas and $D/Dt(\rho_s/\rho) = 0$. Thus the loading does not change as the combustion field unfolds, and if it is initially uniform Eqn. (2) shows that

$$\rho l = \text{constant} . \tag{3}$$

For a fixed particle loading ρ_s / ρ, the absorption length l can be varied by varying the particle size d. We wish to consider the situation where the loading is small yet l has a significant impact on the radiative transport within the combustion field. When l^{-1} is small radiation effects will be negligible and we wish to examine the first effects of finite l^{-1}. As we shall see, there is one effect that is linear in l^{-1} and one that is quadratic. The length against which l is to be measured is the flame-thickness δ in the first case, the flame-radius r_* in the second, so that the two effects can be comparable in magnitude at the same time. The radius of any confinement vessel plays no role.

There is a need for accurate numerical simulations for this problem but we wish to pursue an alternative path, with the goal of unraveling and clarifying various key physical ingredients of the problem. To this end we shall make a number of approximations, for the most part of a rational nature (those that are not are extra-rational modeling simplifications). We shall examine flames of sufficiently large radius that they may be well approximated by a hydrodynamic description. That is, on the scale of the radius r_*, they appear, to good approximation, as discontinuities separating cold gas from hot gas. To leading order in the cold gas

$$T = T_f \quad \text{and} \quad u = W\left(\rho_f / \rho_a - 1\right)\left(r_*^2 / r^2\right) \tag{4}$$

where W is the flame-speed. W is not in general the adiabatic flame-speed but is controlled by flame-stretch and by the radiation effects. The flame-temperature (the temperature at r_* -0) is, to leading order, T_a, with corresponding density ρ_a.

The effects of finite l on this picture are manifest in three ways: Radiation cooling causes the temperature in the burnt gas to drop below T_a; and the flame-speed W is changed by what we shall call the *Spalding effect*, and the *Joulin effect*.

The Spalding effect refers to the diminution in flame-speed that occurs because of heat losses from the flame-structure [3]. The temperature within the structure is governed by an equation of the form

$$M\, C_p\ dT/dx = d/dx\left(\lambda\,(T)\, dT/dx\right) - 4\sigma\, l^{-1}\left(T^4 - T_f^{\,4}\right) + .. \tag{5}$$

where we have only shown convection, diffusion, and radiation terms. The latter has significant impact (changes the flame-speed by O(W) amounts) if

$$B\left(\delta / l_a\right) \sim\ \theta^{-1} \tag{6}$$

where B is the Boltzmann number $4\sigma T_a^{\,4} / M\, C_p\, T_a$, δ is the flame-thickness $\lambda/M\, C_p\left(M = \rho_f W\right)$, l_a is the absorption length evaluated when $\rho = \rho_a$ $\left(l_a >> \delta\right)$, and $\theta \equiv E/RT_a$ is the (large) activation energy characteristic of the global kinetics. The Boltzmann number is also large and we say more about this below.

The Joulin effect refers to the increase in flame-speed that arises because of radiative preheating [4]. Radiation from the hot burnt gas (rather, the particles immersed in that gas) is absorbed by the particles in the cold gas and raises the temperature immediately ahead of the flame. We shall see that this temperature rise is initially of order

$$\Delta T / T_a\ \sim\ B\ \left(r_* / l_a\right)^2 \tag{7}$$

and first has a significant impact when of magnitude ~ θ^{-1}.

Typical values of B are shown in Fig. 1, calculated for lean methane/air mixtures from numerical results of Giovangigli and Smooke [5]. Near-limit mixtures are characterized by large values of B so that examining the estimates (6) and (7) we are naturally led to the distinguished limit defined by

$$\underline{\theta \to \infty}: \; B \sim \theta \, , r_* / l_a \sim \theta^{-1} \, , \; \delta / l_a \sim \theta^{-2} \, , \; \delta / r_* \sim \theta^{-1} \; . \tag{8}$$

Both radiation effects are then comparable in magnitude.

The Spalding effect is non-zero right from the start, and changes only because of changes in the flame thickness associated with changes in M. On the other hand the Joulin effect is initially very small, but grows in importance as the volume of hot burnt gas increases with r_*. Eventually the estimate (7) breaks down when r_* is no longer small compared to l_a. When $r_* >> l_a$ plane flame results are valid and an approximate analysis yields the following formula [6],

$$\Delta T = 2 (T_a - T_f) B / \sqrt{4B^2 + 3} \; . \tag{9}$$

The corresponding flame-temperature is $T_a + \Delta T$ which is significantly larger than T_a so that these flames eventually travel at speeds significantly greater than W_{ad}.*

---

* The plane flame described here is analogous to the excess enthalpy flames described by Weinberg [7] except that the preheating is enhanced by radiation and not by conduction through metal structures.

Note that when B is $O(\theta^{-1})$, Eqn. (9), together with the usual asymptotic result relating flame temperature and speed (see Eq. (25)), implies that

$$M / M_{ad} = \exp\left[\theta\, B\,(T_a - T_f)/(\sqrt{3}\ T_a)\right] \qquad (10)$$

an implicit formula for M (since $B \propto 1/M$) equivalent to one first given in [4] and incorrectly applied in [8] (but with a correct conclusion) to an application where B is not small.

According to the limit defined by (8), the flame-thickness divided by the flame radius is of order $1/\theta$. Asymptotic analysis tells us that stretch effects can then be significant - that stretch alone can cause W to differ significantly from W_{ad}. We shall account for this using Markstein's formula, recently shown by Tseng *et al* to be accurate for our geometry even when the stretch is not weak [9].

The Joulin Effect

In order to describe the Joulin effect we need to calculate the temperature field in both the burnt and fresh gas, and this is the meat of our analysis.

Cold-gas temperature

Radiation cooling in the burnt gas induces an inflow - a correction to the formula (4b) - but we do not believe that it plays an important role in the physics, and so we shall neglect it. Then $O(\theta^{-1})$ deviations of T from T_f are described by

$$\rho_f\, C_p\left[\partial T/\partial t + W\left(\rho_f/\rho_a - 1\right)\left(r_*^2/r^2\right)\partial T/\partial r\right] = -\, r^{-2}\, \partial/\partial r\left(r^2 q_r\right) . \qquad (11)$$

This equation can be integrated along the characteristic $dr/dt = W\left(\rho_f/\rho_a - 1\right)\left(r_*^2/r^2\right)$ with initial conditions $T = T_o$, $r = r_o$ at $t = 0$. A characteristic intersects the flame trajectory and at the intersection point it imposes an $O(\theta^{-1})$ increment in flame temperature which leads to an O (W) change in flame speed. We are only concerned with early times during which the radiative preheating is small and the cold-gas temperature remains close to T_f. Thus emission is unimportant if $T_f = 300$°K, and the only contribution to q_r (the radial component of the radiative heat flux vector) in Eqn. (11) is emission from the hot gas.

In the absence of absorption $\left(r_*/l_f << 1\right)$ q_r falls off like $1/r^2$,

$$\text{i.e.}\quad q_r(r) = q_r(r_*)\left(r_*^2/r^2\right) \text{ in } r > r_* \tag{12}$$

and the term on the RHS of Eqn. (11) vanishes. Then there is no preheating. To account for absorption we adopt a differential-equation (Eddington) approximation for a single outward directed stream of radiation of the form

$$l_f\, r^{-2}\, d/dr\left(r^2 q_r\right) = -a\, q_r \tag{13}$$

where a is constant to be chosen. With the choice a = 1.25 this equation provides a good approximation when the emission from the hot gas is homogeneous (so that the distribution of q_r in the cold gas can be evaluated exactly), and it should work equally well in the general case. Then

$$r^{-2}\, d/dr\left(r^2 q_r\right) = -a l_f^{-1} q_r(r_*)\left(r_*^2/r^2\right)\exp\left[a\left(r_* - r\right)/l_f\right]. \tag{14}$$

The estimate (8b) $\left(r_* / l_a \sim \theta^{-1}\right)$ is a guiding principle for our discussion so that, formally, $r_* / l_f \sim \theta^{-1}$ and the exponential in (14) can be replaced by 1. But for realistic values of θ this is not a good approximation when one recognizes that $l_f / l_a \lesssim 1/5$ so that we shall not make this choice.

Burnt gas temperature and the emitted radiation

If we account only for emission in the burnt gas, the temperature is governed by the equation

$$\rho\, C_p\, \partial T/\partial t \;=\; -\,4\sigma T^4 / l \;, \quad l = l_a T / T_a \;. \qquad (15)$$

Significant cooling occurs on a time

$$\Delta t_{cool} \sim \rho\, l\;\; C_p / \left(4\,\sigma\, T_a^3\right) \qquad (16)$$

and the available time is

$$\Delta t_{avail} \sim r_* / \dot{r}_* \sim \left(\rho_a / \rho_f\right) \left(r_* / W\right) \;. \qquad (17)$$

The ratio of these times $\sim \left(l_a / r_*\right) / B$, an O(1) quantity according to the estimates (8).

Equation (15) is integrated along the characteristic dr/dt = 0 with the initial condition $T = T_a$ when $r = r_*$, consistent with the fact that the flame-temperature differs from T_a by a small $\left(O\left(\theta^{-1}\right)\right)$ amount.

The emitted radiation is calculated by integrating the equation

$$\left(l_a / T_a\right) dI / ds \;=\; \sigma\, T^3 / \pi \qquad (18)$$

over paths that extend from one side of the flame sphere to the other. Then

$$q_r(r_*) = 4\pi r_*^{-2} \int_0^{r_*} dr\, r^2\, \sigma T^4 / \pi l \quad , \tag{19}$$

a quantity that is needed for the calculation of the cold-gas temperature rise. Note that from (11) and (14) we have the estimate

$$\Delta T \sim q_r(r_*)\, \Delta t_{avail} / \left(\rho_f\, C_p\, l_f\right) \quad , \tag{20}$$

and from Eqn. (19) the estimate

$$q_r(r_*) \sim r_*\, \sigma T_a^{\,4} / l_a \tag{21}$$

so that

$$\Delta T / T_a \sim \left(r_* / l_a\right)^2\, \sigma T_a^{\,4} / (M\, C_p\, T_a) \tag{22}$$

as anticipated by Eqn. (7).

An improved description of the burnt gas temperature can be obtained by accounting for absorption, although this is less important than in the cold gas. Then Eqn. (15) is replaced by

$$\rho\, C_p\, \partial T / \partial t = -\, r^{-2}\, \partial / \partial r\, \left(r^2\, q_r\right) \tag{23}$$

where

$$l\, d/dr\, \left(l\, r^{-2}\, d/dr\, \left(r^2\, q_r\right)\right) = 3 q_r + 4 \sigma l\, d/dr\, \left(T^4\right) . \tag{24}$$

Here we use the conventional Eddington approximation, different from the single stream approximation (13).

Numerical Strategy

We have solved the equations using a MacCormack scheme. Standard asymptotic results show that $W \propto \exp\left(-E/2RT_*\right)$ where T_* is the flame temperature, so that

$$M / M_{ad} = \exp\left[\theta\,\Delta T_* / 2T_a\right] \quad (25)$$

where ΔT_* is the increment in flame-temperature over T_a. ΔT_* is small $\left(O\left(\theta^{-1}\right)\right)$ and is the sum of three contributions

$$\Delta T_* = \Delta T_{*_J} + \Delta T_{*_S} + \Delta T_{*_M} \quad (26)$$

where ΔT_{*_J} is generated by the Joulin effect, ΔT_{*_S} (negative) is generated by the Spalding effect, and ΔT_{*_M} is the increment due to flame-stretch.

To account for stretch we use a formula due to Markstein which has recently been shown (empirically) to be accurate in the present geometry for values of stretch that are not small [9]. Specifically,

$$M / M_0 = 1 + C / r_* \quad (27)$$

where M_0 is the flame-speed in the absence of stretch, corresponding to

$$\Delta T_{*_M} / T_a = 2\,\theta^{-1}\,ln\left(1 + C / r_*\right). \quad (28)$$

For the lean methane/air mixtures for which we have done our calculations C is positive.

The drop in flame-temperature due to the Spalding effect is obtained in the usual fashion [10] by integrating the loss term in Eqn. (5) over the flame-structure, at the same time allowing for losses towards the burnt gas (i.e. the non-zero value of $dT/dr\left(r_* - 0\right)$). We assume that $\lambda \sim T^{0.8}$. This yields a formula of the form

$$\Delta T_{*_S} = -\left(M_{ad}^2 / M^2\right) 2T_a Q / \theta \ . \tag{29}$$

Q is a non-dimensional global (but intra-structural) heat loss term. Thus

$$M / M_{ad} = \left(1 + C / r_*\right) \exp\left(\theta \Delta T_{*_J} / 2\, T_a\right) \exp\left[-Q\ M_{ad}^2 / M^2\right] . \tag{30}$$

The Spalding effect changes because of changes in M, but always has the same order-of-magnitude fixed by the particle loading (l) and it slows the flame. The stretch and Joulin effects on the other hand change strongly with time in the sense that the first becomes small and the second starts small. All three have to be updated at each time integration. Stretch enhances the flame speed (since C > O) for small values of r_*, but this effect diminishes as r_* increases. The Joulin effect also enhances the flame-speed, an enhancement that is vanishingly small for small radius, but becomes ever more significant as the radius increases. Note that W (determined by Eqn. (30)) is related to the flame-trajectory slope by

$$\rho_f W = \rho_a \dot{r}_* \ . \tag{31}$$

Results

Specific choices for T_a , W_{ad} and C enable us to simulate methane/air flames. Motivation for this comes from the single experimental record [8]. Values of T_a and W_{ad} are obtained from ref. [5], C from ref. [9]. θ is taken to be 14.3, as proposed in ref. [11]. For initial conditions we started with $r_* = 1.5$ cms and $T = T_a$ in $r < r_*$, $T = T_f$ in $r > r_*$.

Examination of the temperature distribution in the (diffusive) preheat zone assuming $\lambda \sim T^{0.8}$ shows that these flames have thickness less than 3mm so that if the initial flame radius is 1.5 cm the hydrodynamic description that we have adopted is not unreasonable.

Figure 2 shows the variations of burning velocity (W) with time for an equivalence ratio of 0.527 (then $T_a = 1535$ K, $W_{ad} = 5.15$ cm/s) and various values of l_a when stretch and the Joulin effects are accounted for, but the Spalding effect is discarded ($Q = 0$). This is an artificial situation designed to show how strong the Joulin effect is and at what time it becomes significant. When $l_a = 100$ cm, radiation effects are small but large enough that the flame speed always measurably exceeds the adiabatic value. At early times it is substantially greater because of stretch effects. For $l_a = 50$ cm, and smaller, there is a sharp increase in flame speed following the initial decrease.

Figure 3 shows the corresponding variation of r_* with time. Each curve is - more or less - a straight line, with increasing slope as l_a is decreased. The significance of these results is that, according to plane theory, there will eventually be a significant impact on the flame-speed because of radiation (see Eqn. (9)) and this effect should be detectable in the spherical configuration on time and space scales typical of those used in the laboratory.

We do not show results generated when absorption in the burnt gas is not accounted for. When $l_a \geq 30$ cm they do not differ significantly from those shown, but for smaller values of l_a the errors are noticeable, with overprediction of the flame-speed.

In Fig. 4 are shown temperature histories at three different locations when $l_a = 20$ cm (again, for Q = 0). Absent absorption in the burnt gas, the temperature there falls monotonically with time (Eqn. (15)) and this characteristic is preserved when $l_a = 50$ cm over the time scale that we have examined. But for $l_a = 20$ cm the temperature displays a minimum, and this is not difficult to understand. Consider the 3cm history. When the flame passes through this point its temperature is close to the adiabatic flame temperature. There is then significant cooling, since the flame sphere is optically thin, and the temperature drops significantly below T_a. But we know from elementary energy considerations that, as $r_* \rightarrow \infty$ and the plane results are recovered, the temperature far behind the flame must be equal to T_a [6], and so T must, in due course, rise again. Each curve in Fig. 4 would display a minimum at some time, if the time scale were sufficiently extended. Note that the record at the 10 cm mark shows a radiatively induced temperature rise ahead of the flame of about 100K. There is also a measurable rise at the 5 cm mark.

A characteristic of the Spalding effect is that it can quench the flame if Q is large enough. Heat losses sufficient to quench an adiabatic flame may not quench the spherical flame since stretch effects can provide an antidote for small r_*, Joulin effects for large r_*. At the same time, whereas we are assured that a sufficiently large flame can survive - ultimately the Joulin effect dominates - a small flame may not. Figure 5 shows variations of W with time when the Spalding effect is included for values of l_a between 50 cm and 100 cm.

Consider the curve for l_a = 58 cm. There is initially a sharp drop in flame speed due to the diminishing stretch. The flame-speed drops below the adiabatic flame speed because of the Spalding heat losses. But beyond about 0.13 secs it rises because of the Joulin effect. Note that for these flames $l_a / \delta \sim 50$ cm / 2.5 mm ~ 200 which is consistent with the estimate (8c) for when the Spalding effect will be significant.

The situation is quite different when l_a = 55 cm. The flame-speed falls, as before, but before it reaches a minimum quenching occurs. Our model forces us to end the curve at that point. In actuality the flame-speed would fall to zero on the time scale δ/W. The critical value of l_a for which quenching first occurs (here between 57.5 cm and 58 cm) depends on the estimate for Q. When we first did these calculations we used a cold-gas value of λ and, in so doing, underestimated the Spalding loss and predicted a critical l_a of about 12 cm.

Figure 6 shows the corresponding variations of flame-radius with time. For these relatively large values of l_a the Joulin effect has not had time to significantly counteract the Spalding effect and the effective flame-speed monotonically increases with l_a.

These results suggest that quenching due to the Spalding effect is an obstacle to the generation of flames in dusty gases by point ignition unless the ignition kernel can overwhelm the losses until the Joulin effect can dominate.

The Experimental Record and Concluding Remarks

We have examined an unsteady premixed flame generated by point ignition supported by a gas containing an inert dust. This dust emits and absorbs significant amounts of radiative energy and this influences the flame behavior. We have not accounted for the thermal capacity of the dust - the small-loading approximation, justified below. In carrying out this calculation we have made a number of other approximations, listed here:

(i) the flame is a hydrodynamic discontinuity with stretch effects accounted for in a semi-empirical fashion;

(ii) the flame temperature differs only a little from the adiabatic flame temperature, an assumption that is valid for sufficiently small times but does not preclude flame speeds significantly in excess of the adiabatic flame speed when the activation energy is large;

(iii) cooling-induced inflow is neglected;

(iv) Eddington-type approximations to the radiative transport are adopted.

Our results show that for lean methane /air mixtures (e.g. ϕ = .527) the addition of modest amounts of dust should generate noticeable radiative preheating for flames of radius 6-12 cms provided they survive Spalding extinction at small radius. The temperature rise of a particle located immediately ahead of the flame at any time is generated by the history of this particle as it moves outwards from its initial location until the flame catches up with it at that time. This thermal history is independent of any confinement vessel walls. The particle is indifferent to whether the radiation that passes through it unabsorbed is eventually absorbed by other particles or is 'lost' to a wall. Indeed, insofar as the radiation is concerned, a cold non-reflecting wall plays no role. In this connection we disagree with the claim in ref. [8] that the combustion chamber size plays a role.

Reference [8] provides the sole experimental record against which the present results and those for plane flames [4], [6] can be measured. Table 1 shows Planck lengths for different total particle masses calculated for the apparatus of ref. [8]. The mean particle diameter is 0.6 μm and the calculations assume $T_f = 300$ K, $T_a = 1535$ K. The mass of gas is 14.44 gm. The values of m_p marked with a star are nominal experimental values - nominal because these are supply values, and what proportion ended up on the floor of the apparatus, and what was suspended in the gas, is unknown [8]. Note that all flame trajectories were determined from photographic records obtained exterior to the 25 cm diameter containment vessel, so that the smaller values of l_f shown in Table 1 could not have been achieved.

The other values of m_p shown in the table correspond to the values of l_a that we have used in our calculations. Note that for all of these the loading m_p / m_g is small and justifies our neglect of the thermal capacity of the particles.

Table 1

Mass of particles in the combustion chamber, m_p (gm)	m_p / m_g	l_f cm	l_a cm
0.08	0.005	19.55	100.0
0.16	0.011	9.77	50.0
0.25*	0.017	6.32	32.33
0.27	0.019	5.86	30.0
0.40	0.028	3.91	20.0
0.50*	0.035	3.16	16.16
0.62	0.043	2.54	13.0
0.75*	0.052	2.11	10.78
2.0*	0.138	0.79	4.04
7.5*	0.519	0.21	1.08

There are unexplained differences between the experimental record and the theoretical predictions. Thus at the 4.5 cm mark no measurable increase in temperature ahead of the flame due to radiative preheating is reported for $m_p = 0.25$, 0.75 or 2. (There is, however, an increase in the flame temperature for $m_p = 0.25$). For values of r_* greater than ~ 3 cm constant flame speeds are reported and there is no evidence of a growing Joulin effect matching the growth in r_*. At the same time if these measured flame speeds are final values, equivalent to one-dimensional propagation speeds, it should be noted that none of the superadiabatic values predicted by one-dimensional theory are obtained [4], [6]. This lack of agreement is noted in [8].

There is good evidence of a Spalding effect. The addition of 0.25 gm causes a sharp drop in flame speed below the adiabatic value. However, the addition of greater amounts does not cause quenching but generates flame speeds intermediate between the values for 0 gm and 0.25 gm.

The reasons for the discrepancy between theory and experiment are not known at the present.

Acknowledgment

This work was supported by AFOSR and by the NASA-Lewis Research Center.

References

[1] G. Joulin, *Combustion Science and Technology*, 52: 377-395 (1987).

[2] J. Lee, P. Ronney, and K. Seshadri. Private communication.

[3] D.B. Spalding, *Proc. Roy. Soc. London*, 240A: 83-100 (1957).

[4] G. Joulin and B. Deshaies, *Combustion Science and Technology*, 47: 299-315 (1986).

[5] V. Giovangigli and M.D. Smooke, *Combustion Science and Technology*, 87: 241-256 (1992).

[6] J. Buckmaster and T. Jackson, 'Flames in dusty mixtures - their structure and stability', submitted.

[7] F. Weinberg, *15th Symposium (International) on Combustion*, The Combustion Institute, Pittsburgh, pp. 1-17 (1974).

[8] A. Abbud-Madrid and P. Ronney, 'Premixed flame propagation in an optically-thick gas', paper to appear in the *AIAA Journal*.

[9] L.K. Tseng, M.A. Ismail, and G.M. Faeth, 'Laminar burning velocities and Markstein numbers of hydrocarbon/air flames', paper to appear in *Combustion and Flame*.

[10] J. Buckmaster and G.S.S. Ludford, *Theory of Laminar Flames*, Cambridge Press, New York, 1982, p. 43.

[11] P. Ronney, *22nd Symposium (International) on Combustion*, The Combustion Institute, Pittsburgh, pp. 1615-1623 (1974).

Figure Captions

Fig. 1 Variations of the Boltzmann number $4\sigma T_a^4 / MC_p T_a$ with equivalence ratio for methane/air mixtures with M and T_a determined from the adiabatic flame calculations of ref. [5]. Our calculations are for an equivalence ratio of 0.527.

Fig. 2 Variations of burning velocity with time for different Planck lengths when the Spalding effect is neglected (Q = 0) (see Fig. 3).

Fig. 3 Variations of flame radius with time for different Planck lengths when the Spalding effect is neglected (Q = 0) (see Fig. 2).

Fig. 4 Temperature histories at r = 3 cm, 5 cm, and 10 cm when l_a = 20 cm, Q = 0.

Fig. 5 Variations of burning velocity with time for different Planck lengths (see Fig. 6).

Fig. 6 Variations of flame radius with time for different Planck lengths (see Fig. 5).

Fig 1

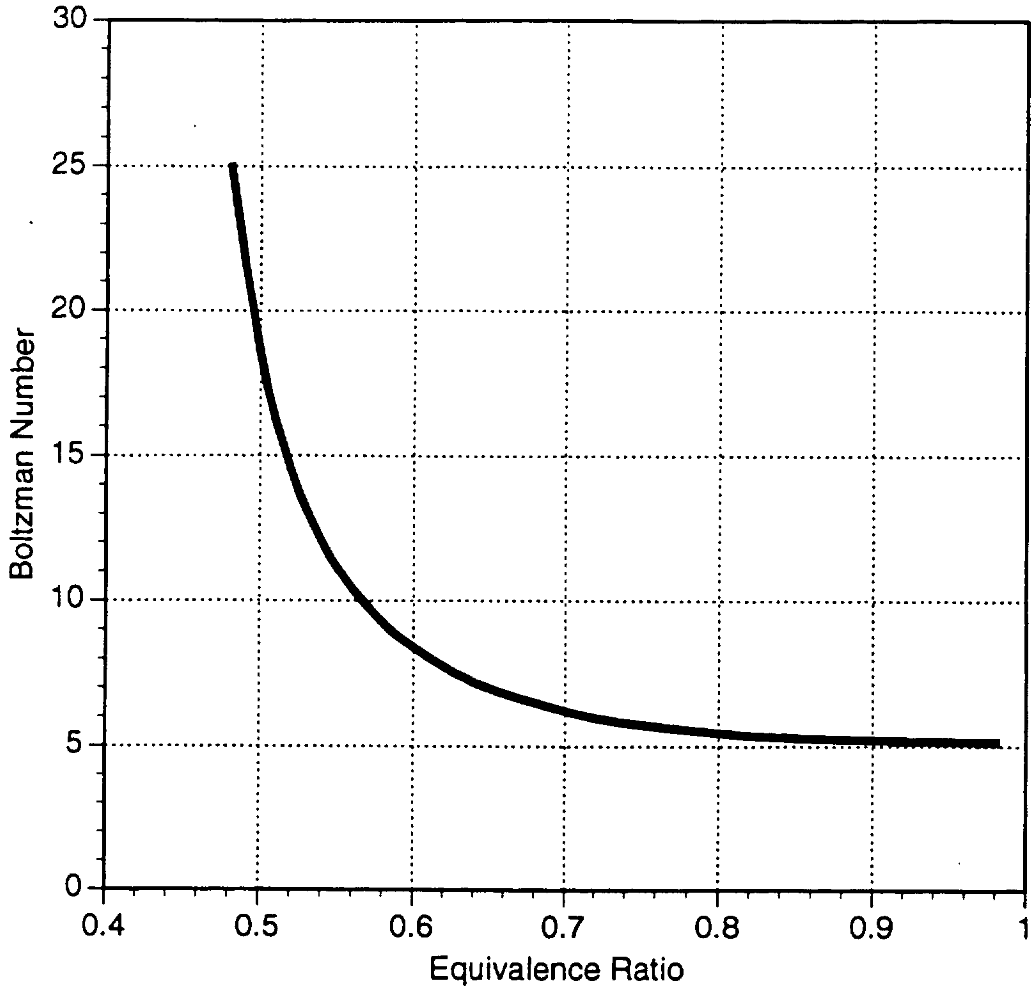

30
25
20
15
10
5
0
Boltzman Number
0.4
0.5
0.6
0.7
0.8
0.9
1
Equivalence Ratio

Fig. ~~3~~ 2 : Variation of burning velocity with time for different optical path lengths

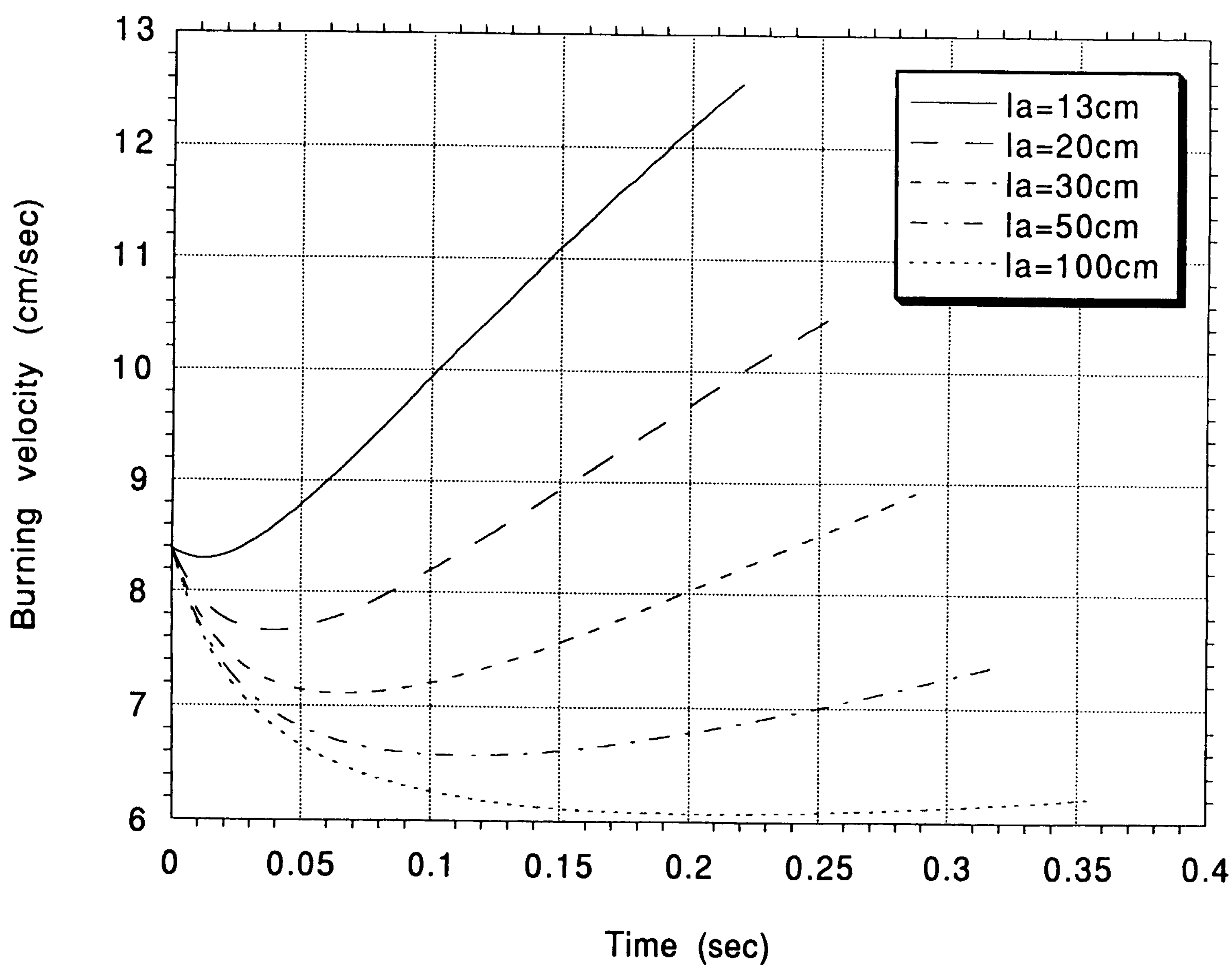

Fig. ~~4~~ 3 : Flame front propagation for different optical path lengths

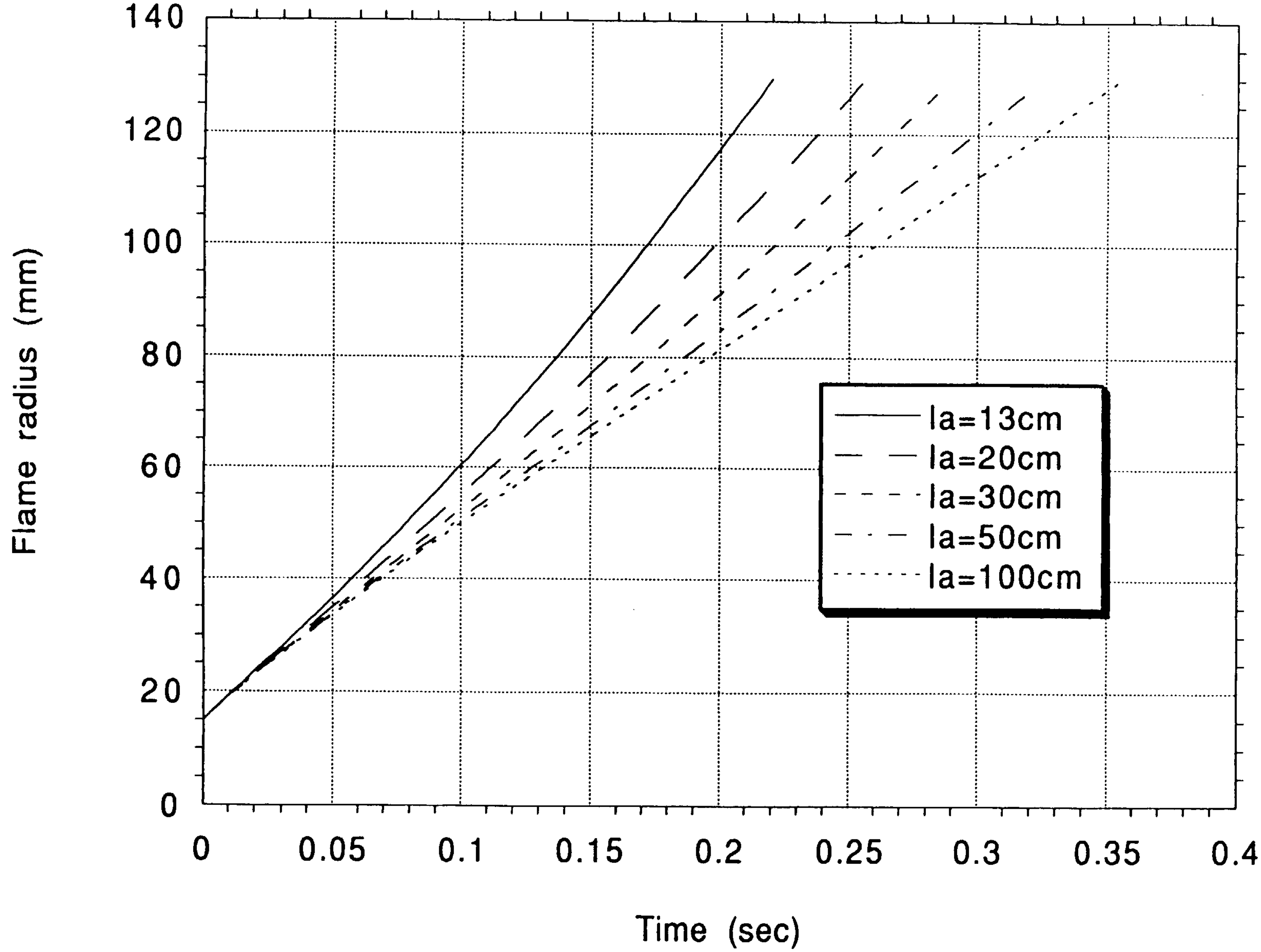

Fig. ~~5~~ 4 : Temperature histories at different locations for la=20cm in 5.25% methane-air mixtures

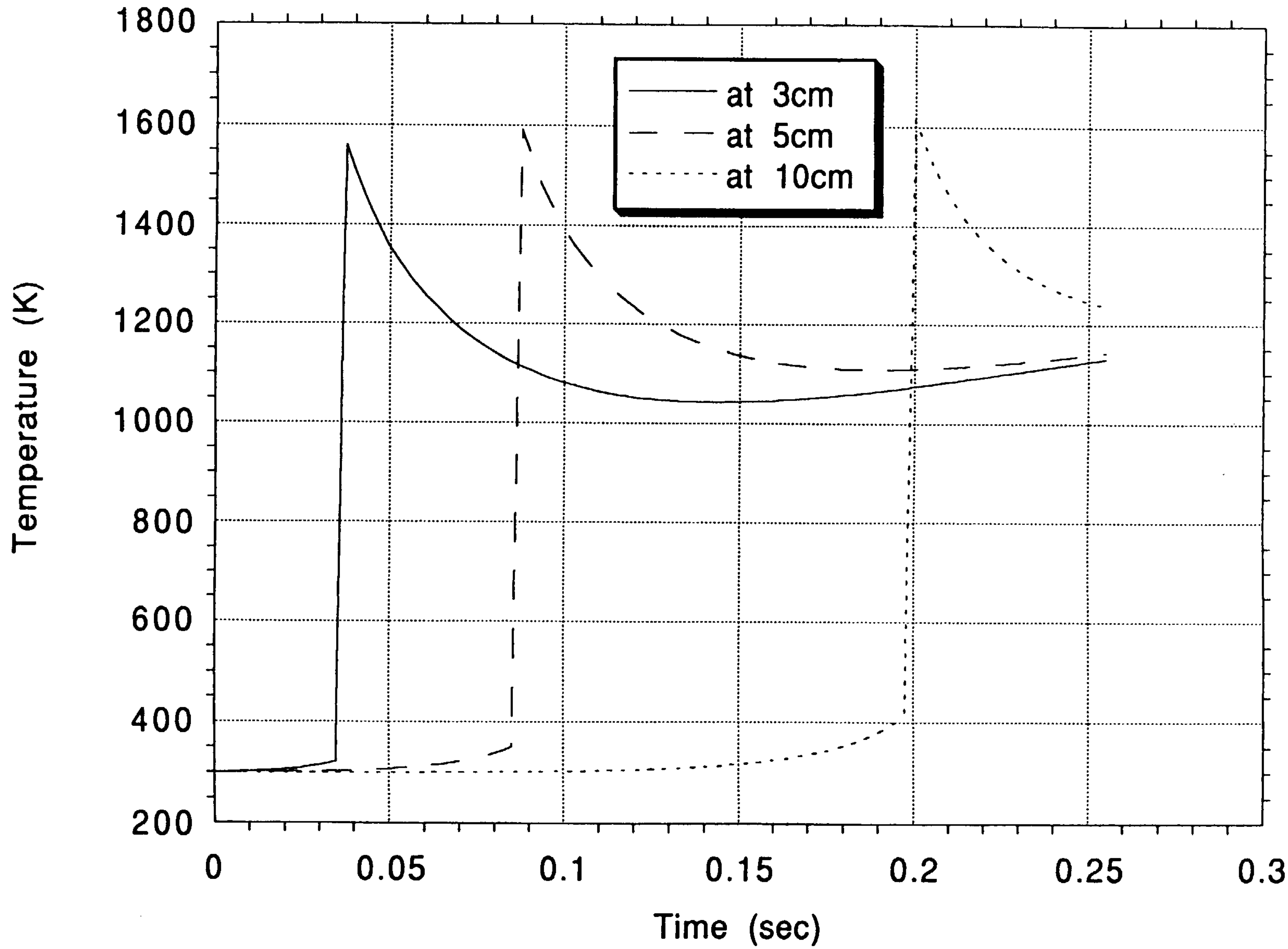

Fig. ~~6~~ 5 : Curves showing extinction of flame for
la < 58cm

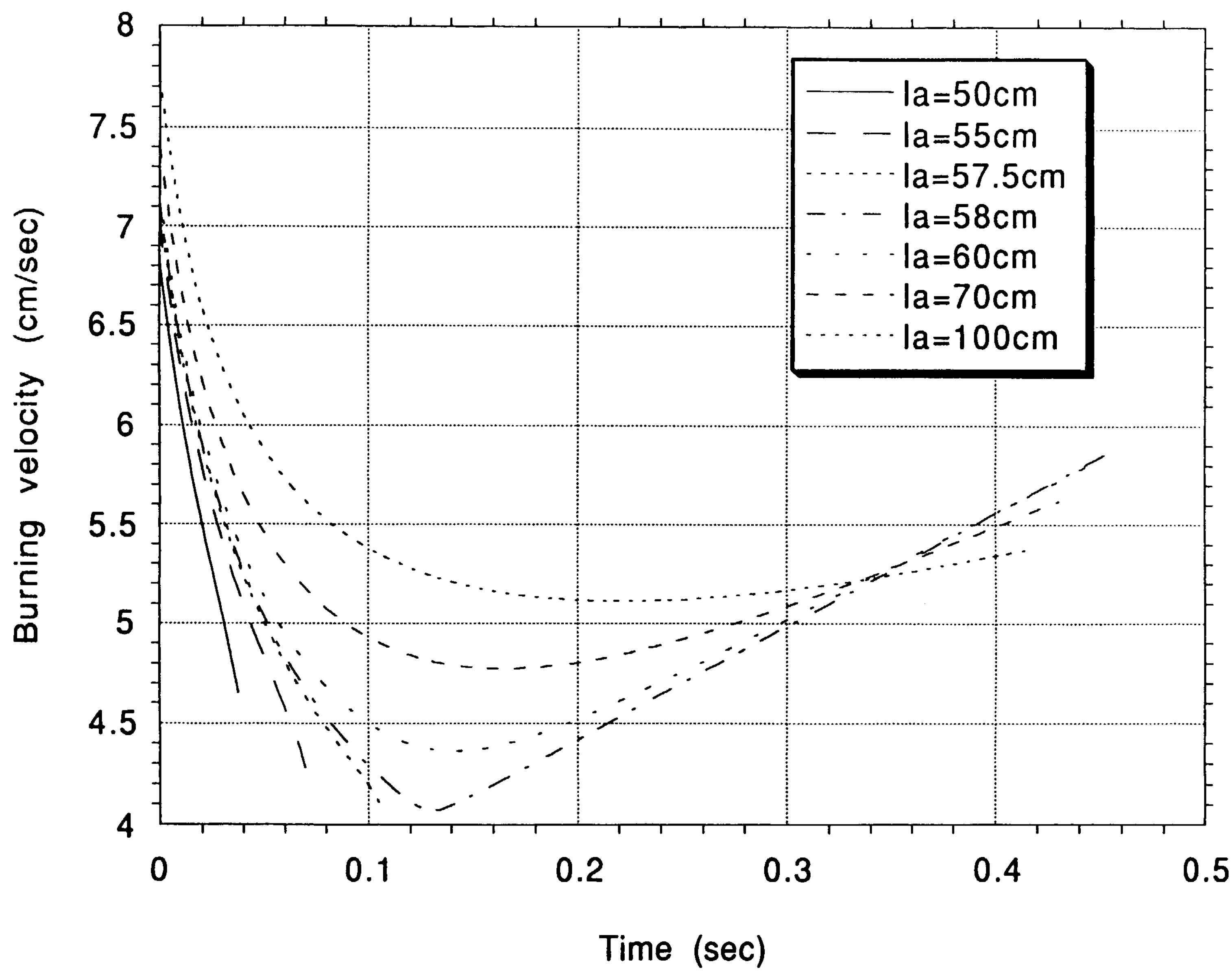

6

Fig. ~~7~~ : Flame front propagation when Spalding heat loss is accounted for